Desalination and Water Treatment
www.deswater.com

doi: 10.5004/dwt.2021.27372

229 (2021) 302–313
July

Selective adsorption of mercury(II) ions from aqueous solution by two kinds of modified cellulose microsphere

Jifu Du[a,c,†], Qi Ye[b,†], Zhen Dong[b], Xin Yang[a], Long Zhao[b,*]

[a]*School of Nuclear Technology and Chemistry & Biology, Hubei University of Science and Technology, Xianning 437100, China*
[b]*State Key Laboratory of Advanced Electromagnetic Engineering and Technology, School of Electrical and Electronic Engineering, Huazhong University of Science and Technology, Wuhan 430074, China, emails: zhaolong@hust.edu.cn/ryuuchou@hotmail.com (L. Zhao)*
[c]*Hubei Key Laboratory of Radiation Chemistry and Functional Materials, Hubei University of Science and Technology, Xianning 437100, China*

Received 16 November 2020; Accepted 26 April 2021

ABSTRACT

Microcrystalline cellulose microsphere was functionalized by using radiation-induced grafting polymerization and following modification. The adsorption performances of the L-cysteine and pentaethylenehexamine functionalized resin (named CysMC and PMC) toward mercury (Hg) were tested by batch experiment. The experimental isotherm data were both well described by the Langmuir isotherm model. The results showed the maximum adsorption capacity for Hg(II) by CysMC and PMC were calculated to be 264.55 and 169.49 mg/g, respectively. The adsorption kinetic data were well fitted by the pseudo-second-order model for both CysMC and PMC. Thermodynamic studies indicated the Hg(II) adsorption was endothermic by CysMC but exothermic by PMC. The selectivity and repeated use were investigated. The two adsorbents can removal Hg(II) from an aqueous solution selectively and good repeated use performance. Moreover, X-ray photoelectron spectroscopy analysis was used to demonstrate the adsorption mechanism.

Keywords: Mercury adsorption; L-cysteine; Pentaethylenehexamine; Radiation grafting; Microcrystalline cellulose

1. Introduction

Mercury (Hg) and its derivatives are acknowledged as one of the most poisonous contaminants due to their toxicity, non-biodegradable and bioaccumulative. Hg mainly comes from industrial, electroplating wastewater, ore industry, fertilizer and medicine factory [1]. Governments from around the world have set regulations of the Hg emission standard and upper limit for Hg(II) in drinking water. For example, the emission standard in Europe, United States and China are set as 50–80 ug/L [2]. The World Health Organization (WHO) has announced an upper limit of 1 ug/L Hg(II) concentration in drinking water and it is 2 ug/L by United States [3]. Because Hg can be accumulated in the human body, which will cause great harm to nature and human beings [4]. So how to remove mercury from wastewater efficiently and quickly has become a widely concerned topic.

At present, the methods of Hg removal include chemical precipitation, solvent extraction, photoreduction, membrane filtration, coagulation, flocculation, ion exchange, and reverse osmosis et al., but those methods sometimes cause secondary pollution to the environment [5]. The adsorption method has been widely studied because of its advantages of simplicity, high efficiency, wide application range, low cost and high selectivity [6]. Many kinds of adsorbents such as metal–organic frameworks [7], graphene oxide composite [8], wool chelating fibers [9], hydrogel [10] had been investigated for Hg removal.

* Corresponding author.

† Both the authors equally contribute to this work.

In recent years the functional groups contain N and S, such as sulfur [11], mercapto [12], thiol [13] and amino groups exhibited an excellent adsorption performance for Hg(II) ions. In the adsorption process, some practical aspects must be considered such as the cost, fabrication processes, large-scale production, ease of use [14], the adsorption selectivity with the coexistence of other heavy metals, regeneration [15]. In this regard, the preparation of the adsorbent particularly the microsphere-based adsorbent (economical, environmental, efficient adsorption performance and can be simply used in the existing adsorption tower) are also important for practical applications.

Cellulose, one of the most abundant and inexpensive natural polymers, has been widely used as an adsorbent matrix for further modification. The modification by functional groups can enhance its adsorption capacity toward metal ions [3]. The abundant hydroxyl provides the sites for free radical grafting polymerization [16,17]. Radiation-induced grafting polymerization (RIGP) had been inclusively investigated to introduce a desirable functional group on the surface of various polymers [18]. The polymer functional groups synthesized in this way are mainly concentrated on the surface, resulting in the high adsorption rate to the target ions [19]. In this paper, two kinds of adsorbents, L-cysteine (Cys) and pentaethylenehexamine (PEHA) functionalized cellulose microspheres were prepared by RIGP and further modification. The adsorption performances and the adsorption mechanism to Hg(II) were studied.

2. Materials and methods

2.1. Materials

Microcrystalline cellulose microspheres (MCC) were obtained from Asahi Kasei Chemicals Corporation, Japan. Pentaethylenehexamine (PEHA), mercury chloride ($HgCl_2$) and glycidyl methacrylate (GMA) were obtained from Macklin Reagent Co., Ltd., (China) L-cysteine and N,N-dimethylformamide (DMF) were obtained from Sinopharm Chemical Reagent Co., Ltd., (China). All reagents are analytical reagents and used directly.

2.2. Preparation of CysMC and PMC

GMA was grafted on MCC microspheres through RIGP technology which procedure can be found in the literature [18,20]. Briefly, a glass reaction kettle in a water bath contains 100 mL GMA emulsion solution (30 wt.% GMA, 3 wt.% Tween 20) was nitrogen bubbled to remove oxygen and heated to 50°C. 10 g MCC was sealed in PE bag and irradiated at a dose of 30 kGy (10 kGy/pass) by EB accelerator at 1 MeV under the condition of dry-ice cooling. The irradiated MCC was then quickly put into the GMA solution and reacted for 2 h. After washed with de-ionized water and dried, MCC-g-GMA was then obtained. The grafting yield calculates by mass increasing was 230%.

MCC-g-GMA was further modified by ring-opening reaction in L-cysteine (DMF solution) and PEHA (aqueous solution). The ring-opening condition was at 80°C for 24 h. Then the microspheres were separated, washed and dried at 40°C. L-cysteine and pentaethylenehexamine functionalized resin (named CysMC and PMC) were obtained. The synthesis route is shown in Fig. 1.

2.3. Characterization

The surface morphologies were characterized using a scanning electron microscope (SEM; Hitachi S-4800). X-ray photoelectron spectroscopy (XPS; AXIS Ultra instrument) was carried out to analyze the sample elements. Fourier-transform infrared spectroscopy (FTIR) instrument was used to study the resins before and after adsorption. The specific surface areas of the resins before and after adsorption were determined by the Brunauer–Emmett–Teller (BET; ASAP2420-4MP, Micromeritics, American) method.

2.4. Adsorption performance

2.4.1. Batch experiments

The mass of 0.01 g CysMC or PMC was immersed in 10 mL of Hg(II) solution for the adsorption experiments. The mixture was stirred at 120 rpm and 25°C. The Hg(II) concentration before and after adsorption was measured by an inductively coupled plasma spectrophotometer (ICP;

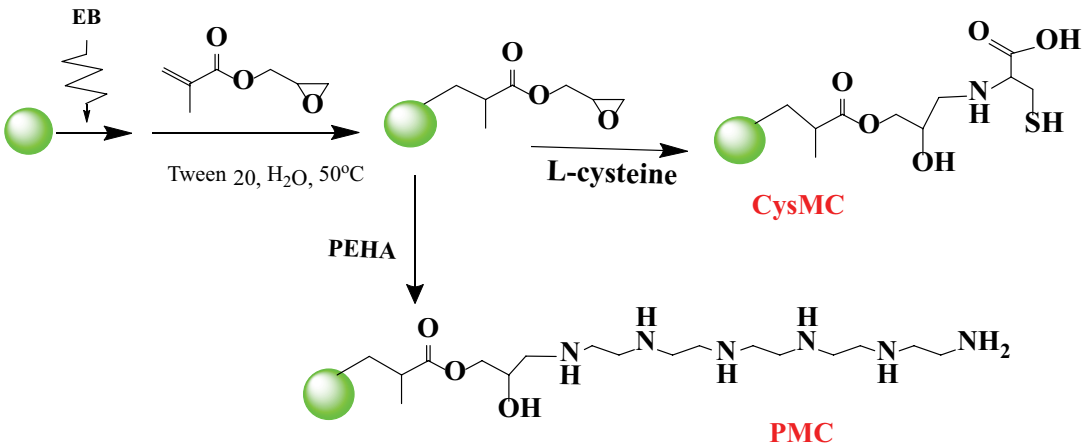

Fig. 1. Procedure for the preparation of PMC and CysMC.

ICPS-7510, SHIMADZU, Japan). All experiments were carried out in three parallel samples, the final results were the average value.

The adsorption capacity (Q_e) and removal efficiency (E%) were defined as follows:

$$Q_e = \frac{(C_0 - C_e)V}{m} \quad (1)$$

$$E\% = \frac{C_i - C_e}{C_i} \times 100 \quad (2)$$

where C_0 and C_e were the initial and equilibrium concentration of Hg(II), respectively. m was the weight of CysMC or PMC and V was the volume of Hg(II) aqueous solution. In the range of pH (1–7), the influence of initial solution pH on the Hg(II) adsorption at 10 mg/L was investigated; adsorption kinetics were conducted with the contact time (5–600 min) and Hg(II) 10 mg/L; adsorption isotherms were conducted with initial Hg(II) concentration (100–300 mg/L) and 24 h; thermodynamics was conducted at optimum pH with the temperature (25°C–40°C) for 24 h. The effect of NaCl was investigated at the Hg(II)/NaCl mole rate 1/(1–1,000). Effect of coexisting metal ions (Cd(II), Cr(III), Mn(II), Pb(II), Co(II), Ni(II) and Zn(II)) with mole ratio 1:1 were studied.

2.4.2. Regeneration and reusability

The regeneration and reusability of CysMC or PMC were tested by adsorption–desorption cycles. After saturated adsorption (0.01 g adsorbents were added into 10 mL 10 mg/L solution with shaking for 24 h), the Hg(II)-loaded-adsorbents were regenerated by using 0.2 mol/L HNO_3 + 0.1 mol/L thiourea as elution solution with the volume 10 mL. After elution, CysMC or PMC were immersed in NaOH solution with pH 12 for 4 h and dried for next adsorption–desorption cycles.

2.4.3. Trace Hg(II) adsorption

0.01 g CysMC or PMC in 10 mL Hg(II) solution with initial concentration 100 ug/L at 25°C for 24 h.

3. Results and discussion

3.1. Characterization

3.1.1. Scanning electron microscopy

Figs. 2a–f show the SEM morphologies of MCC, MCC-g-GMA, and that of CysMC and PMC before and after adsorption. The MCC microsphere was spherical and approximately 100 μm in diameter. The diameter of the MCC-g-GMA microsphere increased significantly to about 200 μm after grafting. The surface became rough. In addition, the diameter of the CysMC and PMC was in the range of 200–250 μm. Similar morphology appeared on the surface of CysMC-Hg and PMC-Hg.

3.1.2. Fourier-transform infrared spectroscopy

The FTIR spectra of CysMC and PMC before and after adsorption are shown in Fig. 3. Several similar peaks appeared in both spectra images of CysMC and PMC, such as (i) the peaks at around 3,384 cm^{-1} which can be ascribed to –OH, (ii) the stretching vibrations of C–O and C = O around 1,054 and 1,728 cm^{-1}, respectively, and (iii) the vibration absorption peak of N–H around 1,637 cm^{-1} [21]. For CysMC, the peaks at 2,531 cm^{-1} were assigned to S–H and 736 and 640 cm^{-1} were characteristic peaks of C–S [20]. The results suggested the successful synthesis of CysMC and PMC. Besides, it was obvious that the movement of those peaks indicated the formation of chemical boned between reactive groups and Hg(II).

3.1.3. Brunauer–Emmett–Teller

The nitrogen adsorption–desorption studies showed that the BET surface areas of CysMC and PMC were 1.0548 and 0.9732 m^2/g, respectively, which were too low to prove the porous structures of CysMC and PMC. After adsorption of Hg, the BET surface areas of CysMC and PMC were 1.6098 and 1.3802 m^2/g, respectively. There was no obvious change of BET surface area after adsorption.

3.2. Effect of pH on the removal efficiency

Solution pH will affect the form of the metal ions and the charge transfer on the solid/liquid interface, so pH plays a significant role in controlling the adsorption process. As shown in Fig. 4, the maximum removal efficiency was found almost not changed at pH 1–7 by CysMC. But for PMC, the maximum removal efficiency was found at pH 2 which reached 95%. So pH 4.3 (nature pH) for CysMC and pH 2 for PMC were selected to evaluate the adsorption performance.

3.3. Adsorption isotherms: effect of initial concentration

The effect of the initial concentration on the adsorption capacity was investigated to analyze the adsorption mechanism and the distribution of Hg(II) between the solution and the adsorbent. The results in Fig. 5a show that Q_e of CysMC and PMC increased with the increase of Hg(II) concentration and eventually stabilized at the equilibrium concentration. The experimental data were fitted with Langmuir and Freundlich isotherm models, in which linear form can be described by Eqs. (3)–(4) [22]:

$$\frac{C_e}{Q_e} = \frac{C_e}{Q_m} + \frac{1}{K_L Q_m} \quad (3)$$

$$\ln Q_e = \ln K_F + \frac{1}{n} \ln C_e \quad (4)$$

where C_e represented the equilibrium concentration (mg/L) of Hg(II), Q_e (mg/g) was adsorption capacity on per gram adsorbent and Q_m was the maximum adsorption capacity

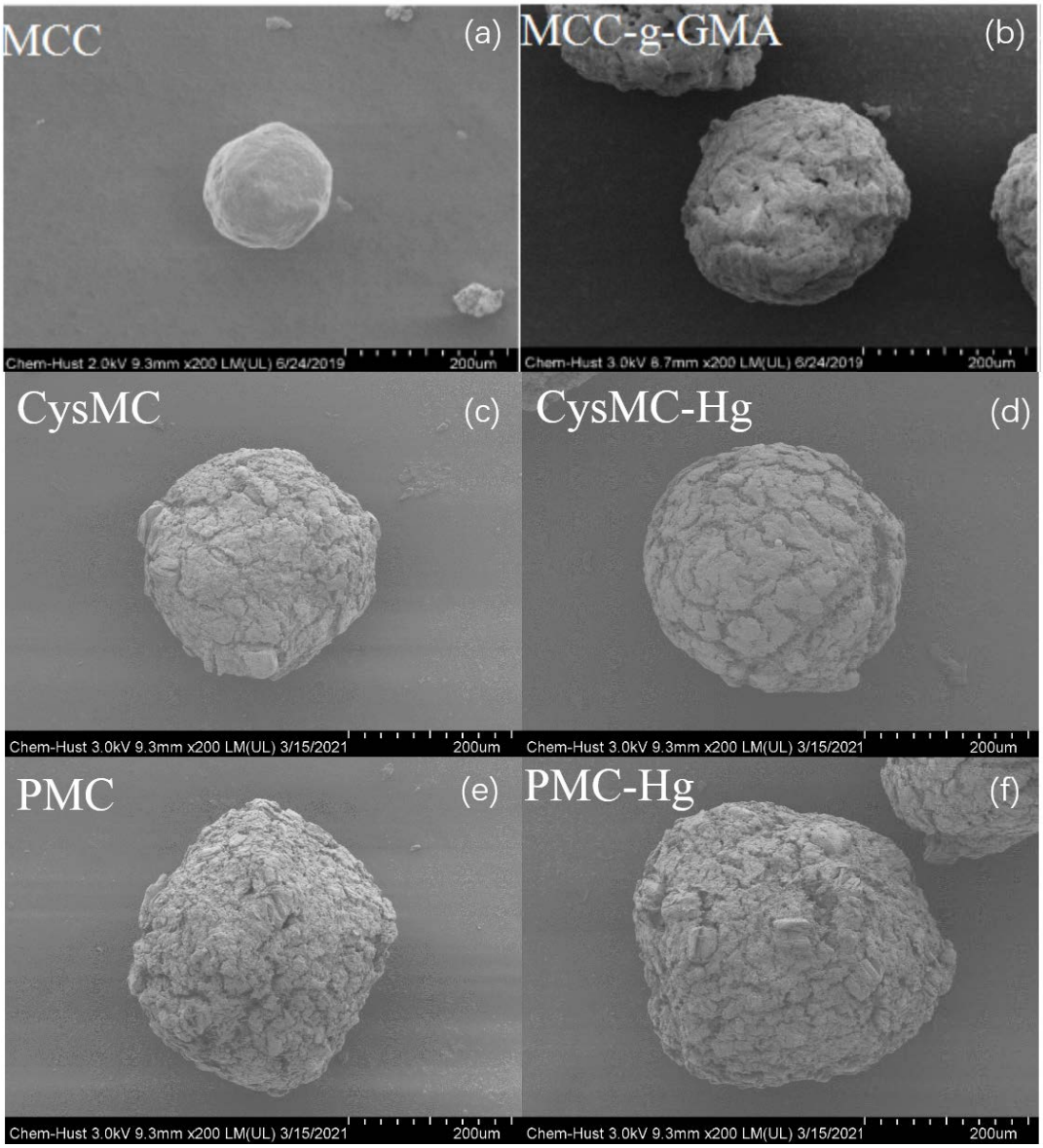

Fig. 2. SEM images of (a) MCC, (b) MCC-g-GMA, (c) CysMC, (d) CysMC-Hg, (e) PMC and (f) PMC-Hg.

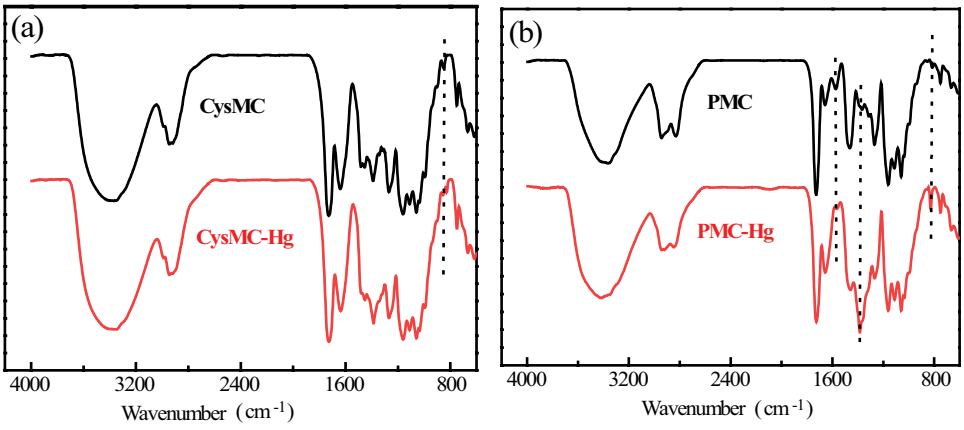

Fig. 3. FTIR spectra of (a) CysMC and (b) PMC before and after adsorption.

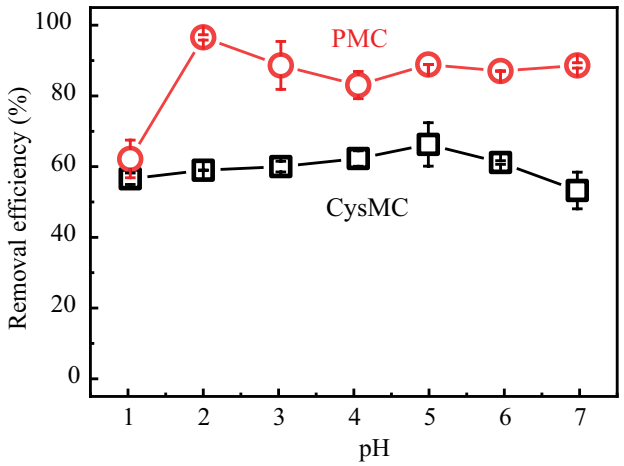

Fig. 4. Effect of pH on the adsorption of Hg(II) onto CysMC and PMC.

(mg/g). K_L and K_F were Langmuir and Freundlich constants, respectively.

Figs. 5b and c show the linear fitting plot of Langmuir and Freundlich model. The key parameters and correlation coefficients were calculated by linear fitting and are summarized in Table 1. Comparatively, the adsorption process can be better described by the Langmuir isotherm model. The high R^2 value (0.9975 and 0.9911 for CysMC and PMC, respectively) of the Langmuir isotherm indicated that the adsorption of Hg(II) formed a single layer onto the surface of CysMC and PMC. The adsorption capacities Q_m of CysMC and PMC were calculated to be 264.55 and 169.49 mg/g, respectively. The adsorption capacities Q_m was much higher than that of other adsorbents given in the Table 2.

3.4. Adsorption kinetics: effect of contact time

The effect of adsorption time on the Hg(II) adsorption is illustrated in Fig. 6a. The Hg(II) adsorption capacity of CysMC and PMC were increased with the increased contact time and finally reached equilibrium. The adsorption kinetics could be described by three models: pseudo-first-order, pseudo-second-order and intraparticle diffusion model models, which are expressed in Eqs. (5)–(7), respectively. Eq. (8) was used to calculate the initial adsorption rate h_0 (mg/g min) ($t \to 0$) [30]:

$$\ln\left(Q_e - Q_t\right) = \ln Q_e - k_1 t \tag{5}$$

$$\frac{t}{Q_t} = \frac{1}{k_2 Q_e^2} + \frac{t}{Q_e} \tag{6}$$

$$Q_t = k_{in} t^{1/2} + I \tag{7}$$

$$h_0 = k_2 Q_e^2 \tag{8}$$

where t was the adsorption time. Q_t and Q_e were the adsorption capacity per gram adsorbent at time t and at the equilibrium time, respectively. I was parameters related to the thickness of the boundary layer. The fitted parameters are shown in Table 3.

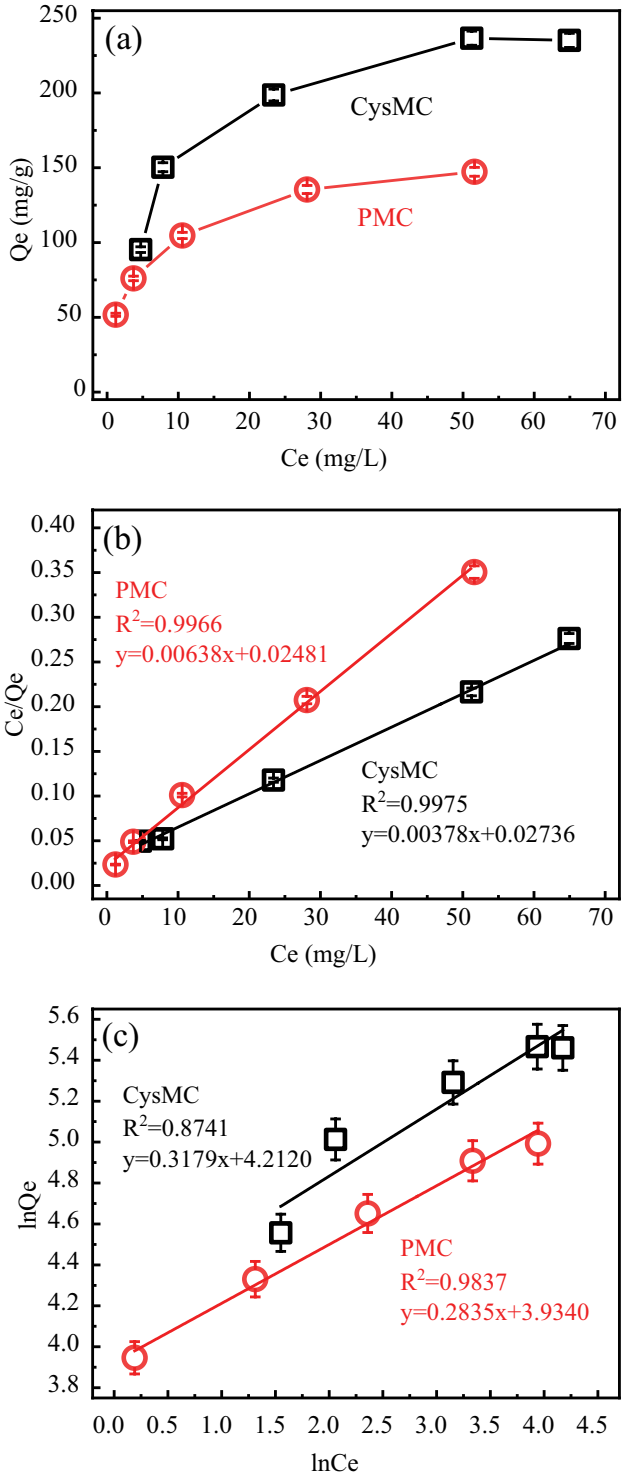

Fig. 5. Equilibrium studies of Hg(II) adsorption: relation of the adsorption capacity with the equilibrium concentration (a), Langmuir isotherm model (b) and Freundlich isotherm model (c).

Table 1
Langmuir and Freundlich isotherm parameters and correlation coefficients for the adsorption of Hg(II)

Adsorbents	Langmuir			Freundlich		
	Q_m (mg/g)	K_L	R^2	K_F (mg/L)	n	R^2
CysMC	264.55	0.1382	0.9975	67.491	3.1457	0.8741
PMC	169.49	0.2482	0.9911	36.867	2.5653	0.9209

Table 2
Comparison of the adsorption capacity of CysMC and PMC with other adsorbent

Adsorbents	Functional group	Q_{max} (mg/g)	Reference
Ti(IV) iodovanadate cation exchanger	Ti(IV) iodovanadate	17.2	[23]
Cellulose	Polypyrrole	31.68	[14]
Bagasse cellulose nanofibers	L-cysteine	116.82	[24]
Wheat straw	—	127.4	[25]
Chitosan/MCM-41-PAA	—	164	[26]
Conjugate nanomaterial	2-Amino-4-chlorobenzenethiol	164.22	[27]
Coal gangue	Mercapto	179.2	[28]
Attapulgite	Polyamidoamine dendrimers	200.8	[29]
Microcrystal cellulose	L-cysteine	264.55	This paper
Microcrystal cellulose	Pentaethylenehexamine	169.49	This paper

Table 3
Kinetic parameters obtained from pseudo-first-order, pseudo-second-order kinetic and intraparticle diffusion models

Model	Parameters	CysMC	PMC
Pseudo-first-order kinetics	k_1 (h^{-1})	1.7931	1.2845
	Q_e (mg/g)	6.3221	9.0413
	R^2	0.8205	0.9769
Pseudo-second-order kinetics	k_2 (g/(mg min))	0.4946	0.2957
	Q_e (mg/g)	6.6304	9.2618
	R^2	0.9997	0.9995
Weber–Morris	h_0	21.744	25.365
	K_{in1}	0.1508	0.1508
	I_{in1}	0.0460	0.0394
	R^2	0.9997	0.9995

Fig. 6b shows the plots of the pseudo-second-order kinetic model. Table 3 shows the linear correlation coefficient (R^2), Q_e, k_1, and k_2. The pseudo-second-order model described the kinetic data well, suggesting the Hg(II) adsorption by CysMC and PMC was a chemical adsorptions process. The intraparticle diffusion model was used commonly to study the transportation of the dissolved contaminants from the solution to the adsorbent. In Fig. 6c the line obtained was not straight, but shows multiply distinct regions. And the first linear part did not pass through the origin, showing that intraparticle diffusion was not the only sole rate-determining step [31].

3.5. Thermodynamics: effect of temperature on adsorption

Temperature is an important parameter that affects the adsorption process. The three main thermodynamic parameters such as a change in free energy (ΔG), enthalpy (ΔH), and entropy (ΔS) were determined at a temperature 300 K, 308 K, 318 K, and 328 K. The thermodynamic parameters were evaluated by Eqs. (9)–(10) [20]:

$$\ln K_L = \frac{\Delta S}{R} - \frac{\Delta H}{RT} \tag{9}$$

$$\Delta G = \Delta H - T\Delta S \tag{10}$$

where K_L is the equilibrium constant obtained from the ratio of adsorbate on the polymer (Q_e) to the adsorbate in the solution (C_e) in the equilibrium state.

Fig. 7 shows the linear plot of thermodynamics. The slope and intercept were obtained through the linear

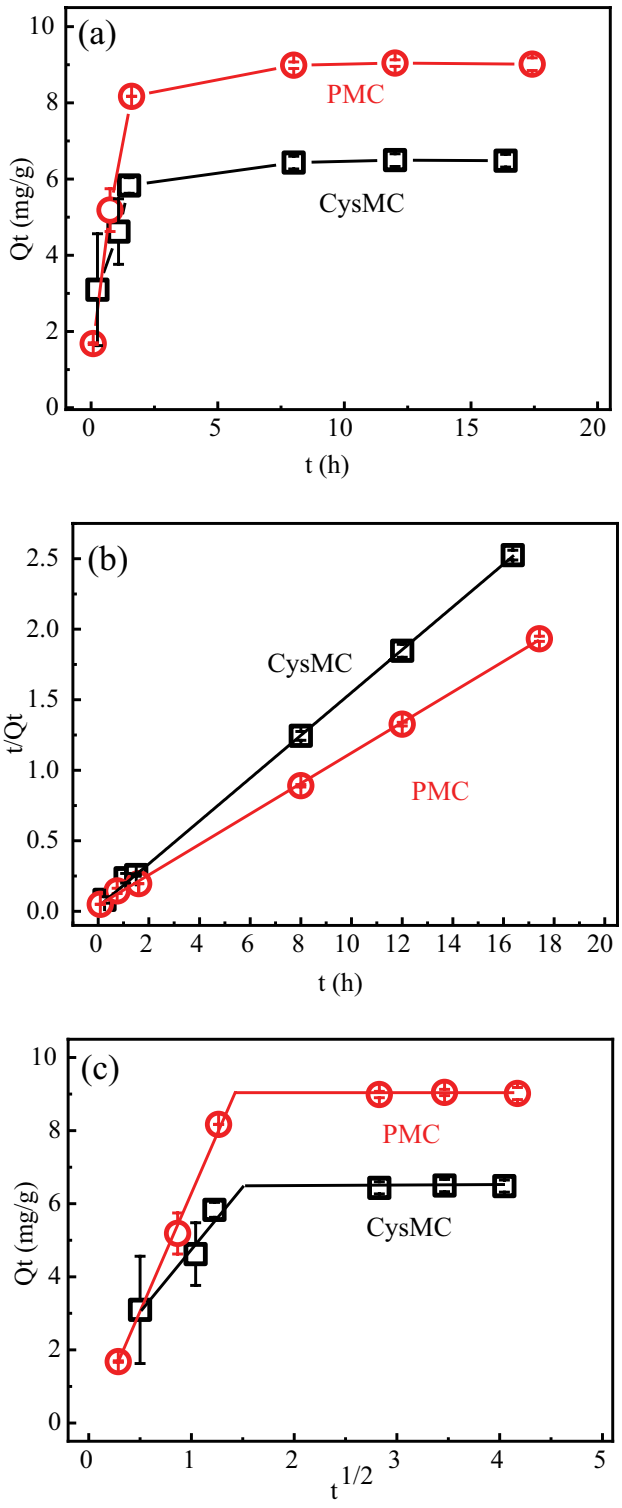

Fig. 6. Adsorption kinetics of Hg(II) on CysMC and PMC: influence of adsorption time (a), pseudo-second-order kinetic (b) and intraparticle diffusion model (c).

fitting, and the ΔH, ΔS and ΔG values at different temperatures can be calculated accordingly, and are listed in Table 4. For CysMC adsorbent, $\Delta H > 0$, $\Delta S > 0$, means the adsorption process was endothermic and can occur

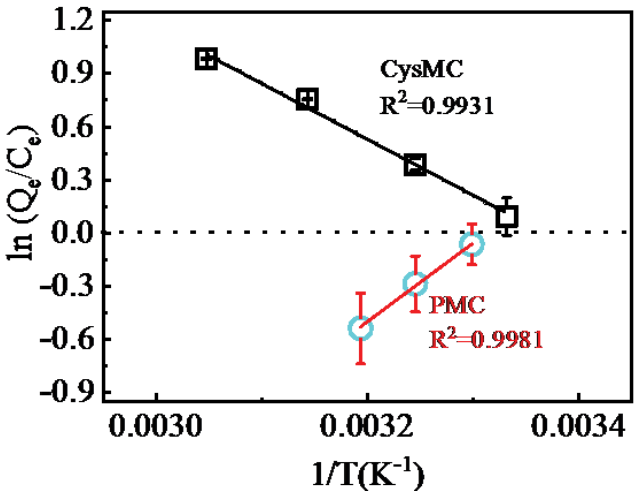

Fig. 7. Thermodynamic plots for Hg(II) adsorption on CysMC and PMC.

spontaneously. $\Delta G < 0$ and ΔG decreases gradually as temperature increases, which means spontaneous nature. For PMC adsorbent, $\Delta H < 0$, $\Delta S < 0$, implied an chemical exothermic properties for Hg(II) adsorption by PMC. $\Delta G > 0$ and with the increase of temperature, ΔG increased gradually, demonstrating that low temperature is beneficial to this reaction.

3.6. Effect of NaCl concentration

The effect of NaCl: Hg concentration ratio on adsorption was investigated with Hg concentration 10 mg/L. According to the results shown in Fig. 8, the adsorption capacity changed slightly due to the existence of NaCl, manifesting that the increasing of NaCl concentration have negligible influence on the adsorption even at the Hg: NaCl = 1:1,000.

3.7. Selectivity: effect of coexisting metal ions

The influence of coexisting metal ions on Hg(II) adsorption was investigated. The experiment was divided into two groups, the first group of coexisting ions contains Hg(II), Cd(II), Co(II), Cr(III), Mn(II), Ni(II), Pb(II) and Zn(II), the second group of coexisting ions contains Ca(II), Na(I), Mg(II) and Cd(II). The mole ratio was 1:1:1:1:1:1:1:1. The distribution coefficient K_d was used to measure the selectivity of the metal ions adsorption on CysMC and PMC, which is described by Eq. (11) [20]:

$$K_d = \frac{C_e}{Q_e} \tag{11}$$

where C_e and Q_e mean the metal ions concentration and adsorption capacity after equilibrium adsorption. Tables 5 and 6 list the distribution coefficient (K_d) for the two groups of the coexisting ions by CysMC and PMC. It can be seen that both CysMC and PMC have higher K_d for Hg(II) than other metal ions, meaning high Hg(II)

Table 4
Thermodynamic parameters of the adsorption of Hg(II) on CysMC and PMC

Adsorbents	ΔH (kJ mol^{-1})	ΔS (J mol^{-1} K^{-1})	ΔG (kJ mol^{-1})			
CysMC	26.469	89.097	T = 300 K	T = 308 K	T = 318 K	T = 328 K
			–0.2320	–0.9909	–1.9962	–2.6849
PMC	–37.429	–123.95	T = 303 K	T = 308 K	T = 313 K	
			0.1619	0.7361	1.4025	

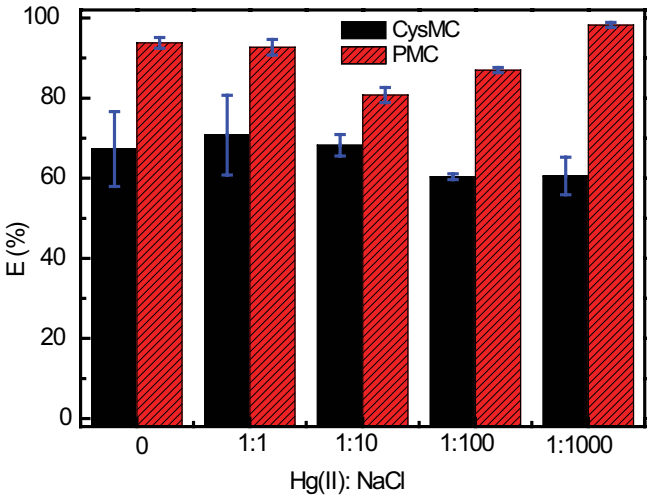

Fig. 8. Effect of Hg(II): NaCl ratio on the adsorption of Hg(II) onto CysMC and PMC.

Table 5
Distribution coefficient K_d for metal ions by CysMC and PMC

Adsorbent	CysMC	PMC
Hg(II)	1,893.4	10,983
Cd(II)	10.472	0.0008
Co(II)	10.637	23.358
Cr(III)	1.835	14.922
Mn(II)	2.955	0.0001
Ni(II)	131.88	0.7927
Pb(II)	16.44	25.56
Zn(II)	5.579	27.45

Table 6
Distribution coefficient K_d for other coexisting ions by CysMC and PMC

Adsorbent	CysMC	PMC
Hg(II)	2,407.2	7,5278
Cd(II)	0.97	9.97
Ca(II)	67.38	1.98
Na(I)	154.9	186.1
Mg(II)	3.62	1.61

selectivity. The adsorption affinity of Hg(II) to CysMC and PMC is stronger than that of other metal ions, especially for PMC, the value $K_d > 10^4$, which showed a very high selectivity performance for Hg(II). The value K_d was 75,278 with the coexistence of Ca(II), Na(I), Mg(II) and Cd(II) ions, which was higher than 10,983 with the coexisting ions Hg(II), Cd(II), Co(II), Cr(III), Mn(II), Ni(II), Pb(II) and Zn(II), which means that PMC had higher selectivity with the coexistence of Ca(II), Na(I), Mg(II) and Cd(II).

3.8. Desorption efficiency and reusability

The adsorption and desorption performance was one of the most important factors to consider the suitability of a material for use as an adsorbent. A mixing solution of 0.2 mol/L HNO_3 + 0.1 mol/L thiourea was tested for elution of the adsorbed Hg(II). The results of five consecutive adsorption–desorption cycles are shown in Fig. 9. For CysMC, the removal efficiency of the first was low, but it increased after elution several times used HNO_3 and thiourea. This maybe because the amine group of CysMC was activated by protonation at lower pH. For PMC, the removal efficiency remained almost constant for the first four-cycle use, and a decrease slightly for the last five-cycle use. So the results proved that CysMC and PMC were suitable for repeated use.

3.9. Trace level adsorption

The adsorption ability of Hg(II) at trace level concentrations was very important because even trace amount can cause very serious environmental problems. 10 mg CysMC and PMC were added into 100 ug/L solutions at natural pH 4.3, the Hg(II) concentration was decreased to 32 and 67 ug/L shown in Fig. 10, which shows that CysMC and PMC have adsorption ability at trace level.

3.10. Adsorption mechanism

The XPS analyses were used to investigate the change of binding energy of N1s and S2p. Fig. 11a shows the wide spectra of CysMC before and after Hg(II) adsorption. The elements C, N, O and S were detected on the surface of CysMC and Hg signal appeared after Hg(II) adsorption, which confirmed the successful adsorption of Hg(II) on CysMC. High-resolution XPS spectra of N1s S2p and O1s are shown in Figs. 11b–d. Before adsorption, N1s peaks were located at 399.67 and 397.9 which were attributed to $-NH_2^+$ and −NH. After adsorption, the N1s

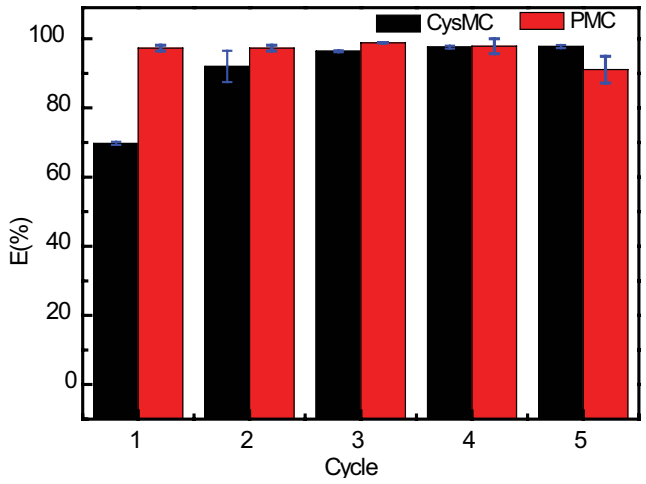

Fig. 9. Adsorption–desorption cycles of CysMC and PMC for Hg(II).

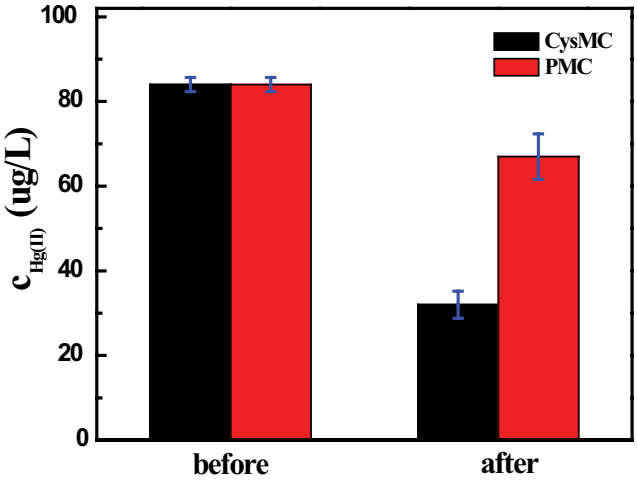

Fig. 10. Hg(II) adsorption at trace level.

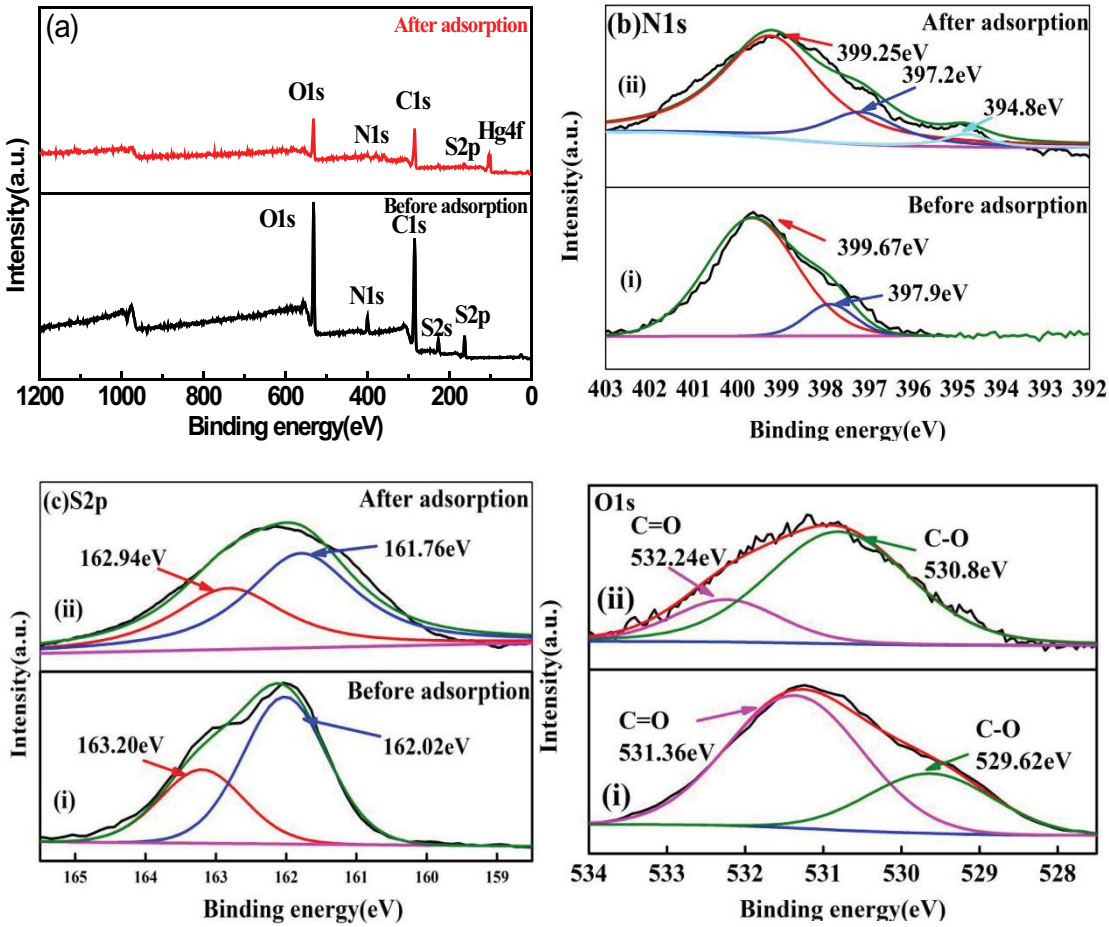

Fig. 11. XPS spectra of CysMC wide scan (a), high-resolution spectra for N1s (b), S2p (c) and O1s (d).

peak was shifted to 399.25 and 397.2 eV [20]. A little peak was located at 394.8 eV, which was corresponding to N–Hg. Before adsorption, two peaks at 162.02 and 163.20 eV were attributed to S2p1/2 and S2p3/2 [32]. After adsorption, the two peaks were slightly decreased and shifted to 161.80 and 162.85 eV. It can be concluded that both –SH and –NH– groups on CysMC played an important role in the adsorption of Hg(II) [24].

Fig. 12 illustrates the chemical bonding configurations of PMC before and after Hg adsorption. In the wide

spectra, the elements C, N and O were detected on the surface of PMC and Hg signal appeared after Hg(II) adsorption, which confirmed the successful adsorption of Hg(II) on PMC. High-resolution XPS spectra of N1s and O1s are shown in Figs. 12b and c. N1s peaks were located at 400.55 eV and 398.7 which corresponded to $-NH_2^+$ and –NH. After adsorption, N1s peaks were was shifted to 400.75 and 399.1 eV. The O1s peaks were located at 532.15 eV, after adsorption, the peak shifted to 531.94 eV and a new peak at 534.6 eV appeared. It can be concluded that –NH– and –OH

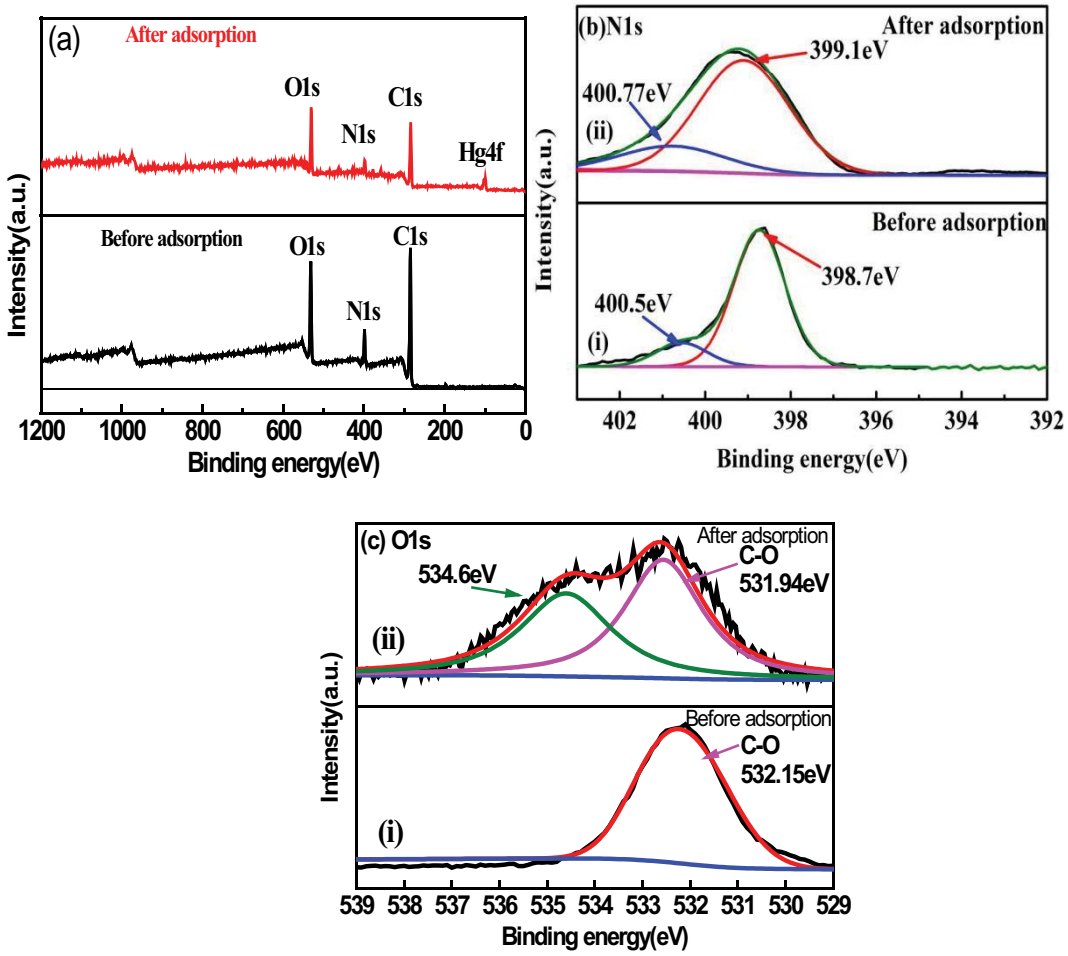

Fig. 12. XPS spectra of PMC: wide scan (a), high-resolution spectra for N1s (b) and O1s (c).

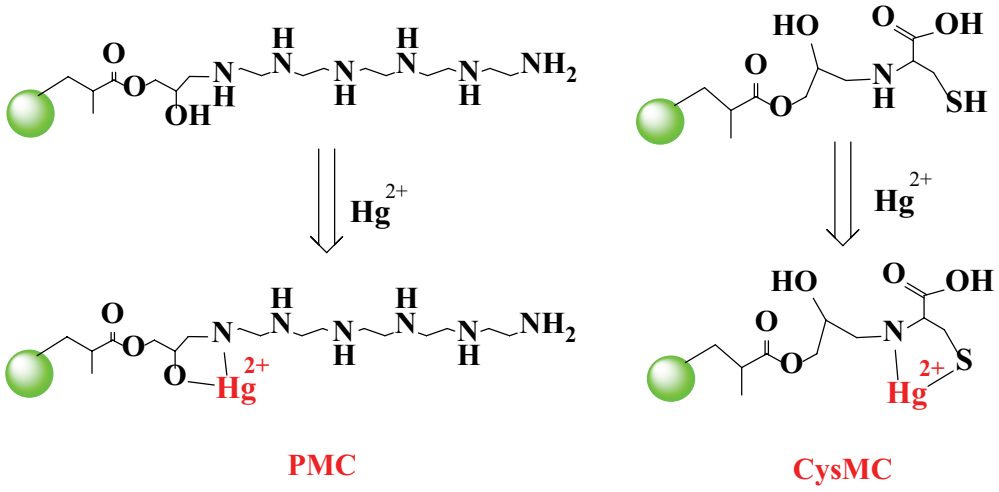

Fig. 13. Mechanism of the adsorption of Hg(II) ion onto CysMC and PMC.

groups on PMC play an important role in Hg(II) adsorption. The adsorption mechanism of Hg by –NH– and –OH groups was also reported in reference [33]. The possible mechanism of the adsorption of Hg(II) ion onto CysMC and PMC is shown in Fig. 13.

4. Conclusion

In this paper, two kinds of adsorption materials with different functional groups, CysMC and PMC, were synthesized by irradiation grafting technique. They have a good adsorption rate, high selectivity and excellent reuse rate for Hg(II) in wastewater, among which the adsorption rate of PMC reached 95%. The isotherm showed that CysMC and PMC resin have higher maximum adsorption capacity, which was 264.55 and 169.49 mg/g, respectively. The experimental isotherm data fitting was more consistent with the Langmuir model, suggesting that there was monolayer adsorption. The kinetic experiments showed that the time to reach adsorption equilibrium was relatively short, and it was in accordance with the pseudo-second-order kinetic model, indicating that the mercury absorption process of the two resins was chemical adsorption. Thermodynamic experiments showed that the mercury absorption process of CysMC resin was an endothermic reaction, and that of PMC was an exothermic reaction. CysMC and PMC have high selectivity for Hg(II) with the coexistence of Cr(II), Co(II), Cr(III), Mn(II), Ni(II), Pb(II) and Zn(II) in the mixing solution. The elution experiment also showed that CysMC and PMC resin have high reuse rates. The adsorption mechanism of Hg(II) by CysMC and PMC was related to the S, N atoms in CysMC and O, N atoms in PMC. Both the two adsorbents showed excellent performance for Hg(II) and is a promising adsorbent.

Acknowledgments

This work was supported by the Hubei Provincial Natural Science Foundation of China (2020CFB852), National Natural Science Foundation of China (11875138, 11905070).

References

[1] S. Kabiri, D.N.H. Tran, S. Azari, D. Losic, Graphene-diatom silica aerogels for efficient removal of mercury ions from water, ACS Appl. Mater. Interfaces, 7 (2015) 11815–11823.
[2] X.X. Liu, X.J. Liu, M.L. Tao, W.Q. Zhang, A highly selective and sensitive recyclable colorimetric Hg^{2+} sensor based on the porphyrin-functionalized polyacrylonitrile fiber, J. Mater. Chem. A, 3 (2015) 13254–13262.
[3] A. Hashem, A.J. Fletcher, M. El-Sakhawy, L.A. Mohamed, S. Farag, Aminated hydroximoyl camelthorn residues as a novel adsorbent for extracting Hg(II) from contaminated water: studies of isotherm, kinetics, and mechanism, J. Polym. Environ., 28 (2020) 2498–2510.
[4] M.H. Zhao, Z. Huang, S.X. Wang, L.B. Zhang, Y. Zhou, Design of L-cysteine functionalized UiO-66 MOFs for selective adsorption of Hg(II) in aqueous medium, ACS Appl. Mater. Interfaces, 11 (2019) 46973–46983.
[5] F.T. Liu, W.J. Xiong, X.R. Feng, G. Cheng, L. Shi, D.W. Chen, Y.B. Zhang, Highly recyclable cysteamine-modified acid-resistant MOFs for enhancing Hg(II) removal from water, Environ. Technol., 41 (2020) 3094–3104.
[6] M.D. Xia, Z.X. Chen, Y. Li, C.H. Li, N.M. Ahmad, W.A. Cheema, S.M. Zhu, Removal of Hg(II) in aqueous solutions through physical and chemical adsorption principles, RSC Adv., 9 (2019) 20941–20953.
[7] L. Esrafili, M. Gharib, A. Morsali. Selective detection and removal of mercury ions by dual-functionalized metal–organic frameworks: design-for-purpose, New J. Chem., 43 (2019) 18079–18091.
[8] Y.X. Ma, P.Q. La, W.J. Lei, C.P. Lu, X.Y. Du, Adsorption of Hg(II) from aqueous solution using amino-functionalized graphite nanosheets decorated with Fe_3O_4 nanoparticles, Desal. Water Treat., 57 (2015) 5004–5012.
[9] M. Monier, D.M. Ayad, A.A. Sarhan, Adsorption of Cu(II), Hg(II), and Ni(II) ions by modified natural wool chelating fibers, J. Hazard. Mater., 176 (2010) 348–355.
[10] G. Yan, S.P. Oliver, Adsorption of Hg(II) from aqueous solution using functionalized hydrogel loaded with hydrous manganese dioxide particles, Water Sci. Technol., 76 (2017) 747–753.
[11] L.J. Huang, Q. Shuai, Facile approach to prepare sulfur-functionalized magnetic amide-linked organic polymers for enhanced Hg(II) removal from water, ACS Sustainable Chem. Eng., 7 (2019) 9957–9965.
[12] S.Y. Bao, K. Li, P. Ning, J.H. Peng, X. Jin, L.H. Tang, Highly effective removal of mercury and lead ions from wastewater by mercapto amine-functionalised silica-coated magnetic nano-adsorbents: behaviours and mechanisms, Appl. Surf. Sci., 393 (2017) 457–466.
[13] S.Y. Xia, Y. Huang, J.C. Tang, L. Wang, Preparation of various thiol-functionalized carbon-based materials for enhanced removal of mercury from aqueous solution, Environ. Sci. Pollut. Res. Int., 26 (2019) 8709–8720.
[14] Z. Hanif, S. Lee, G.H. Qasim, I. Ardiningsih, J.-A. Kim, J.Y. Seon, S.H. Han, S.W. Hong, M.-H. Yoon, Polypyrrole multilayer-laminated cellulose for large-scale repeatable mercury ion removal, J. Mater. Chem. A, 32 (2016) 12425–12433.
[15] W. Liu, X. Zhao, T. Wang, J. Fu, J.R. Ni, Selective and irreversible adsorption of mercury(II) from aqueous solution by a flower-like titanate nanomaterial, J. Mater. Chem. A, 34 (2015) 17676–17684.
[16] R. Kumar, R.Kr. Sharma, Synthesis and characterization of cellulose based adsorbents for removal of Ni(II), Cu(II) and Pb(II) ions from aqueous solutions, React. Funct. Polym., 140 (2019) 82–92.
[17] Z.Y. Wang, M.Q. Lin, Z.X. Dong, J. Zhang, Z.H. Yang, Synthesis and radiation grafting modification of hydroxyl controlled AM/HEMA polymer microspheres, J. Dispersion Sci. Technol., (2020), doi: 10.1080/01932691.2020.1730887.
[18] Z. Dong, J. Zhao, J. Du, C.C. Li, L. Zhao, Radiation synthesis of spherical cellulose-based adsorbent for efficient adsorption and detoxification of Cr(VI), Radiat. Phys. Chem., 126 (2016) 68–74.
[19] J.F. Du, Z. Dong, X. Yang, L. Zhao, Facile fabrication of sodium styrene sulfonate-grafted ethylene-vinyl alcohol copolymer as adsorbent for ammonium removal from aqueous solution, Environ. Sci. Pollut. Res., 25 (2018) 27235–27244.
[20] X. Yang, Q. Pan, Y.Y. Ao, J.F. Du, Z. Dong, M.L. Zhao, L. Zhao, Facile preparation of L-cysteine–modified cellulose microspheres as a low-cost adsorbent for selective and efficient adsorption of Au(III) from the aqueous solution, Environ. Sci. Pollut. Res., 27 (2020) 38334–38343.
[21] Y. Xiong, Y. Song, Q. Tong, P. Zhang, Y.J. Wang, Z.N. Lou, F. Zhang, W.J. Shan, Adsorption-controlled preparation of anionic imprinted amino-functionalization chitosan for recognizing rhenium(VII), Sep. Purif. Technol., 177 (2016) 142–151.
[22] S. Hao, Z.Q. Jia, Intensified adsorption of cesium by PVDF-g-caffeic acid/Prussian blue/polytetrafluoroethylene sandwich membranes, Desal. Water Treat., 181 (2020) 362–368.
[23] Mu. Naushad, Z.A. ALOthman, Md.R. Awual, M.M. Alam, G.E. Eldesoky, Adsorption kinetics, isotherms, and thermodynamic studies for the adsorption of Pb^{2+} and Hg^{2+} metal ions from aqueous medium using Ti(IV) iodovanadate cation exchanger, Ionics, 21 (2015) 2237–2245.

[24] M. Bansal, B. Ram, G.S. Chauhan, A. Kaushik, L-cysteine functionalized bagasse cellulose nanofibers for mercury(II) ions adsorption, Int. J. Biol. Macromol., 112 (2018) 728–736.
[25] R.H. Li, Y.C. Zhang, H.X. Deng, Z.Q. Zhang, J.J. Wang, S.M. Shaheen, R. Xiao, J. Rinklebe, B.D. Xi, X.S. He, J. Du, Removing tetracycline and Hg(II) with ball-milled magnetic nanobiochar and its potential on polluted irrigation water reclamation, J. Hazard. Mater., 384 (2020) 121095, doi: 10.1016/j.jhazmat.2019.121095.
[26] Y. Fu, Y. Huang, J.S. Hu, Preparation of chitosan/MCM-41-PAA nanocomposites and the adsorption behaviour of Hg(II) ions, R. Soc. Open Sci., 5 (2018) 171927, doi: 10.1098/rsos.171927.
[27] Md.R. Awual, Md. Munjur Hasan, G.E. Eldesoky, Md.A. Khaleque, M.M. Rahman, Mu. Naushad, Facile mercury detection and removal from aqueous media involving ligand impregnated conjugate nanomaterials, Chem. Eng. J., 290 (2016) 243–251.
[28] Z.B. Shang, L.W. Zhang, X.Y. Zhao, S.H. Liu, D.L. Li, Removal of Pb(II), Cd(II) and Hg(II) from aqueous solution by mercapto-modified coal gangue, J. Environ. Manage., 231 (2019) 391–396.
[29] W. Qin, G.Y. Qian, H.B. Tao, J.W. Wang, J.Y. Sun, X.F. Cui, Y.G. Zhang, X.L. Zhang, Adsorption of Hg(II) ions by PAMAM dendrimers modified attapulgite composites, React. Funct. Polym., 136 (2019) 75–85.
[30] A.H. Mahvi, M. Sarmadi, D. Sanaer, H. Abdolmaleki, Removal of lead ion from aqueous solutions by adsorption onto phosphate-functionalized treated waste papers (PF-TWPs), Desal. Water Treat., 200 (2020) 205–216.
[31] H. Esfandian, S. Ghanbari Pakdehi, M. Cattallany, Development of a novel method for sodium azide removal from aqueous solution using amberlite IRA-900: batch and column adsorption studies, Desal. Water Treat., 193 (2020) 381–391.
[32] X.H. Wang, R.Z. Sun, C.Y. Wang, pH dependence and thermodynamics of Hg(II) adsorption onto chitosan-poly(vinyl alcohol) hydrogel adsorbent, Colloids Surf., A, 441 (2014) 51–58.
[33] S.A. Ali, I.Y. Yaagoob, M.A.J. Mazumder, H.A. Al-Muallem, Fast removal of methylene blue and Hg(II) from aqueous solution using a novel super-adsorbent containing residues of glycine and maleic acid, J. Hazard. Mater., 369 (2019) 642–654.